Crack-Tip Parameters in Polycrystalline Plates with Soft Grain Boundaries

Yuping Wang[1]; Roberto Ballarini[2]; and Gregory J. Rodin[3]

Abstract: Two micromechanical models are used to calculate the statistical distributions of the stress intensity factor of a crack in a polycrystalline plate containing stiff grains and soft grain boundaries. The first is a finite-element method based Monte Carlo procedure where the microstructure is represented by a Poisson–Voronoi tessellation. The effective elastic moduli of the uncracked plate and the stress intensity factor of the cracked plate are calculated for selected values of the parameters that quantify the level of elastic mismatch between the grains and grain boundaries. It is shown that the stress intensity factor is independent of the expected number of grains, and that it can be estimated using an analytical model involving a long crack whose tip is contained within a circular inhomogeneity surrounded by an infinitely extended homogenized material. The stress intensity factor distributions of this auxiliary problem, obtained using the method of continuously distributed dislocations, are in excellent agreement with those corresponding to the polycrystalline microstructure, and are very sensitive to the position within the inhomogeneity of the crack tip. These results suggest that fracture toughness experiments on polycrystalline plates can be considered experiments on the single grain containing the crack tip, and in turn reflect the a/w effects typical of finite-geometry specimens.

DOI: 10.1061/(ASCE)0733-9399(2008)134:1(100)

CE Database subject headings: Cracking; Plates; Parameters; Grains, material; Finite element method.

Introduction

This paper is concerned with the effects of grain boundary softening on the stress intensity factors of a crack in a plate comprised of columnar grains assumed to be in a state of plane deformation. The study is motivated by the results and analyses reported by Dempsey et al. (1999), who performed in situ fracture toughness experiments on specimens of warm lake ice whose in-plane linear dimension, L, was in the range $0.34 \leqslant L \leqslant 28$ m [Fig. 1(a)]. The average grain diameter of these specimens was $d=15$ cm, so that the number of grains per length was $2 \leqslant L/d \leqslant 200$. Their data, reproduced in Fig. 1(b), indicate the possibility of a size-dependent fracture toughness (defined by the quasibrittle fracture community as the fracture energy "size-effect"). Dempsey et al. rationalized the size effect by the presence of nonlocal inelastic deformation mechanisms that could arise at temperatures, $T \geqslant -4\,^{\circ}\mathrm{C}$, that are "very, very close" to the melting temperature. It should be noted that a significant time period elapsed between preparation and testing of the specimen corresponding to the largest size, and for this specimen a large thermal crack was discovered a few meters ahead of the crack, oriented perpendicular to the main crack path.

While ice grains retain their stiffness at temperatures close to melting, grain boundaries become soft (Barnes et al., 1971; Gandhi and Ashby 1979) and may significantly affect the specimen stiffness. As shown in this paper, the elastic mismatch between the grains and the grain boundaries also results in a strong dependence of the stress intensity factor on the crack-tip location. In situations when the process zone is much smaller than the grain size, which is common to ice, the apparent fracture toughness is expected to be strongly influenced by microstructural features in the vicinity of the crack tip. In particular, consider a crack tip in an ice plate, whose tip is located at some point within a grain. If the grain boundaries are much more compliant than the grains, then the plate response becomes heterogeneous. In this context, it is meaningful to consider the grain containing the crack tip as the fracture specimen, while the remaining grains should be considered as part of the loading device. As a result, the crack-tip stress intensity factor will experience either shielding or antishielding, depending on its position within the grain. The situation can be explained in terms of the classical a/w effect associated with a crack in a finite size specimen, whose stress intensity factor is given in the form, $K_I=\sigma\sqrt{\pi a}F(a/w)$. The soft grain boundaries, in effect, require us to define a and w with respect to the grain containing the crack tip, rather than the entire specimen. This microscopic definition of a and w results in statistical effects on the apparent fracture toughness, based on their corresponding macroscopic values and the overall elastic constants. This paper is concerned with quantifying this effect.

The stress intensity factor of a crack in a polycrystalline plate with soft grain boundaries, K_I^{loc}, [Fig. 2(a)] differs significantly from the apparent stress intensity factor, K_I^{ref}, of a crack in a plate with effective elastic constants equal to those of the homogenized

[1]Developer, FE Technology Integration, Dassault Systemes Simulia Corp., 166 Valley St., Providence, RI 02909.

[2]Professor, Dept. of Civil Engineering, Univ. of Minnesota, 142 Civil Engineering Bldg., 500 Pillsbury Dr. S.E., Minneapolis, MN 55455 (corresponding author). E-mail: broberto@umn.edu

[3]Professor, Dept. of Aerospace Engineering and Engineering Mechanics, The Univ. of Texas at Austin, Austin, TX 78712.

Note. Associate Editor: Bojan B. Guzina. Discussion open until June 1, 2008. Separate discussions must be submitted for individual papers. To extend the closing date by one month, a written request must be filed with the ASCE Managing Editor. The manuscript for this paper was submitted for review and possible publication on October 27, 2006; approved on April 23, 2007. This paper is part of the ***Journal of Engineering Mechanics***, Vol. 134, No. 1, January 1, 2008. ©ASCE, ISSN 0733-9399/2008/1-100–109/$25.00.

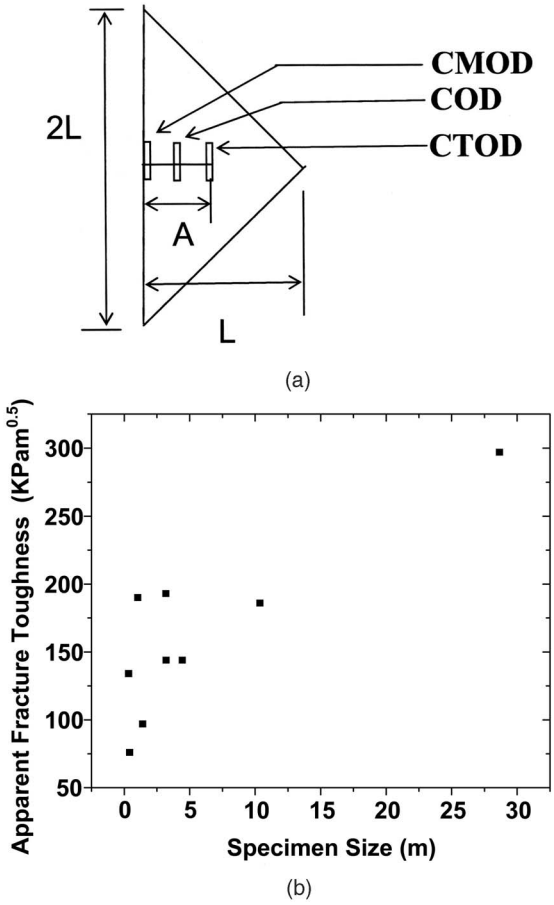

Fig. 1. (a) Warm lake ice specimen indicating crack length, A, in-plane linear dimension, L, and points of crack opening displacement measurements; (b) apparent fracture toughness-specimen size data

polycrystalline plate [Fig. 2(b)]. The fracture toughness reported in Fig. 1(b) represents the critical value of K_I^{ref} at crack initiation, $K_{\text{Ic}}^{\text{ref}}$, which implicitly reflects the condition that K_I^{loc} is equal to the fracture toughness of the material in the immediate vicinity of the crack tip, $K_{\text{Ic}}^{\text{loc}}$. Therefore, the question arises of whether the data is in fact size dependent, or if its large variation merely reflects the statistical distribution of K_I^{loc} produced by grain boundary-induced crack-tip shielding/antishielding. The plausibility of this second explanation is supported by the very large differences in the effective elastic moduli, E_{eff}, (Table 1) that Dempsey inferred by relating the applied load to measurements of crack opening displacements at two points [labeled *COD* and *CMOD* in Fig. 1(a)].

Adopting, as a possible explanation of the data, the size independent fracture view, we propose that a polycrystalline fracture mechanics specimen can be regarded as a single-grain specimen loaded through a metal–ice composite testing machine (Fig. 3). The metal part is the conventional loading machine, and the ice part is what remains of the specimen upon removal of the grain containing the crack tip. In other words, the specimen's apparent fracture toughness, $K_{\text{Ic}}^{\text{ref}}$, does not represent the fracture toughness of the ice grain, $K_{\text{Ic}}^{\text{loc}}$. The correlation between $K_{\text{Ic}}^{\text{loc}}$ and $K_{\text{Ic}}^{\text{ref}}$ requires micromechanical models that capture the effects of initial crack-tip position, such as the ones presented here. They enable correlation between apparent fracture toughness and grain

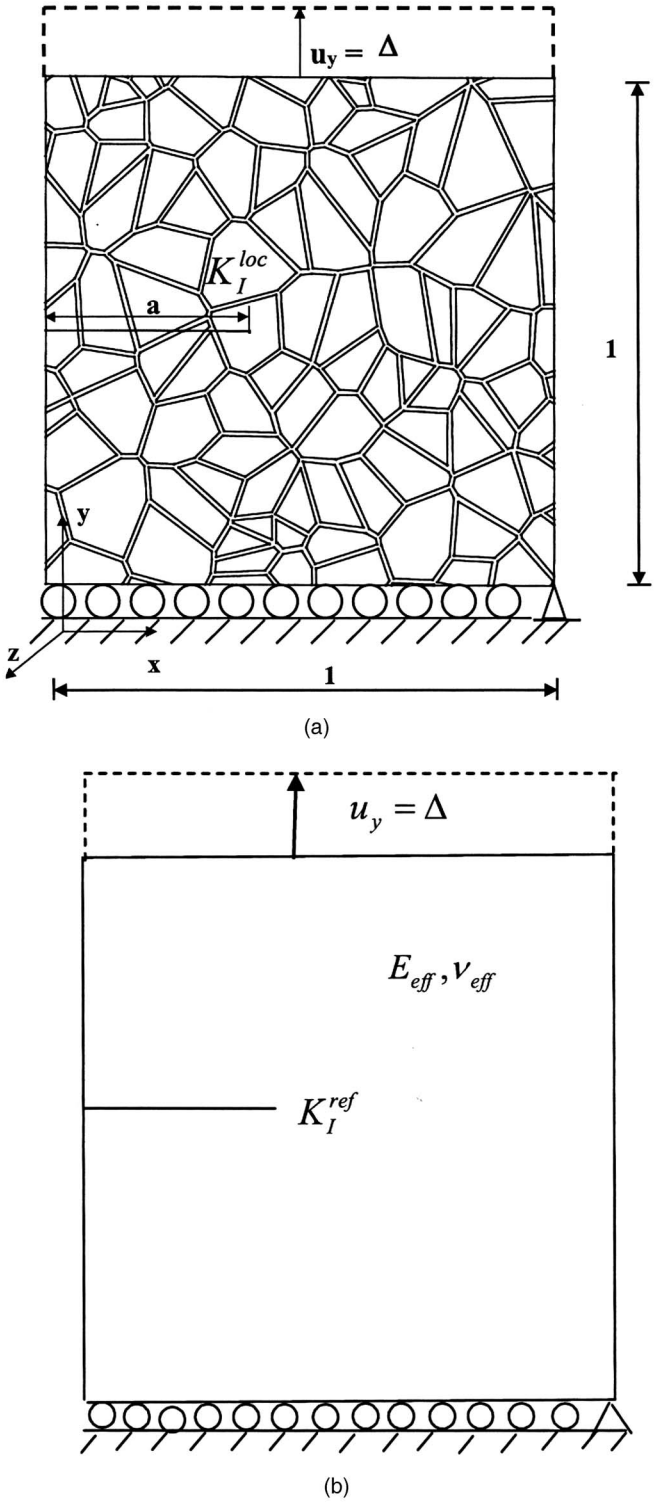

Fig. 2. (a) Crack in polycrystalline plate containing grain boundaries; (b) crack in elastically homogeneous plate

fracture toughness, and in turn prediction of critical fracture loads.

In the next section, a micromechanical model is presented for calculating the effective elastic moduli of polycrystalline plates containing grain boundaries. These serve as the reference elastic constants for the finite-element method based stress intensity factor analysis of a cracked polycrystalline plate and for the analyti-

Table 1. Effective Elastic Modulus of Warm Lake Ice Inferred from Crack Opening Displacement Measurements

Test number	Size (m)	E_{COD} (GPa)	E_{CMOD} (GPa)
1	0.34	—	—
2	0.41	—	5.7
3	1.04	2.8	—
4	1.41	3.5	4.3
5	3.18	—	2.9
6	3.20	3.6	8.0
7	4.42	5.7	7.6
8	10.36	7.7	3.2
9	28.64	10.0	—

cal model of a simplified configuration, presented in the following section. The models are applied to the analysis of warm lake ice apparent fracture toughness data in the last section.

Effective Elastic Moduli

The effective elastic moduli of the polycrystalline plate were determined using a finite-element method based Monte Carlo procedure that simulates loading of the two-dimensional micromechanical model shown in Fig. 4, whose boundaries are defined by $x=0$, $x=1$, $y=0$, $y=1$. This unit area was obtained by cutting the middle of a square area double its size constructed using a method based on Poisson–Voronoi tessellation (Voronoi 1908; Mullen et al., 1997), that is summarized as follows: (1) the expected number of grains per unit area, n, is specified (the expected number of grains in the enlarged area is $2n$); (2) for each of m Monte Carlo realizations, a Poisson variate n_i is generated from the Poisson distribution, with expected value $2n$; (3) a Poisson–Voronoi tessellation containing n_i grains is constructed by first generating n_i randomly distributed nuclei within the doubled area, r_j, $j=1,n_i$. All the points that are closer to r_j than to any other nuclei are defined to comprise the jth of n_i Voronoi cells, whose average linear dimension is d; (4) Interphases of thickness δ are introduced by subtracting a distance of $\delta/2$ from

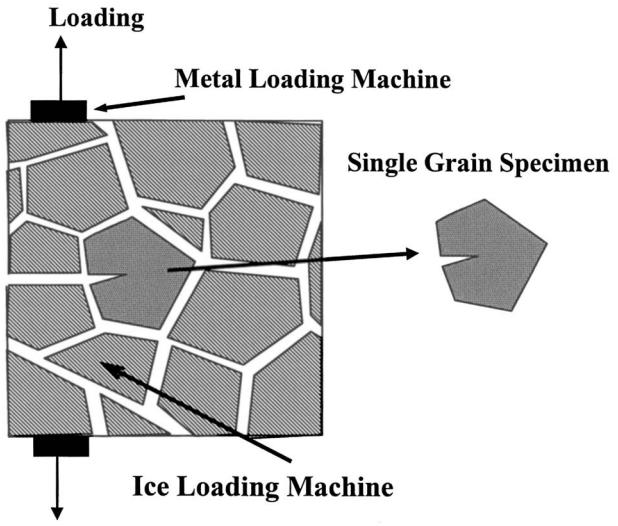

Fig. 3. Metal–ice composite testing machine

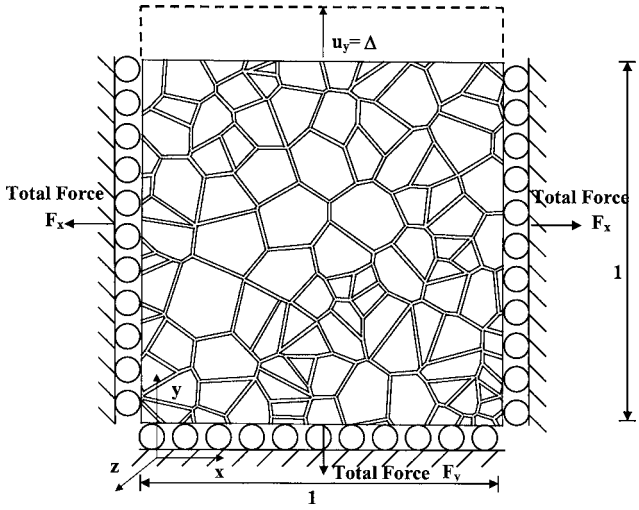

Fig. 4. Micromechanical model for effective elastic constants

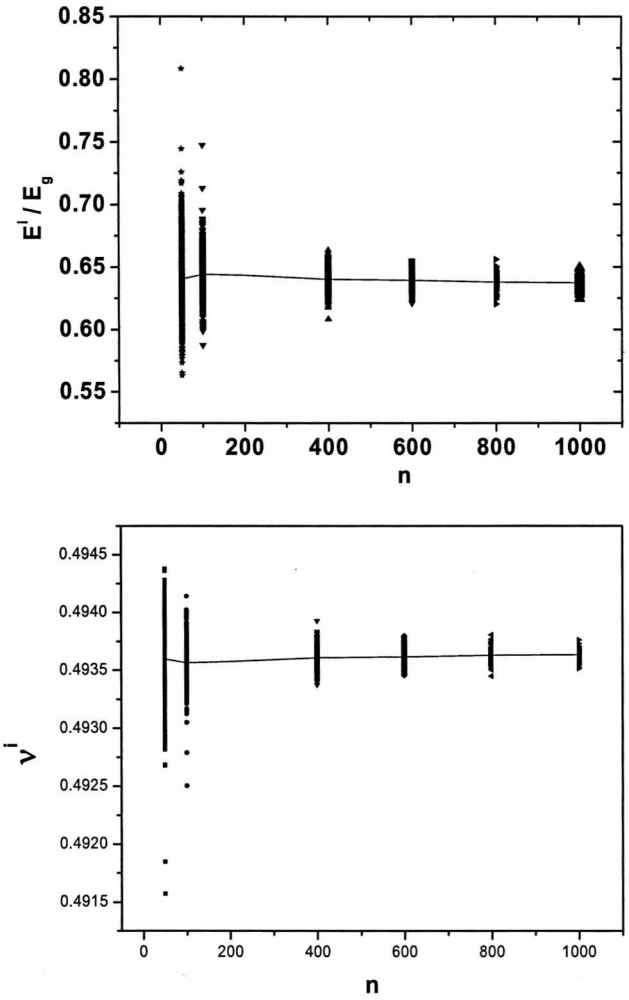

Fig. 5. Scatter of effective Young's modulus, E^{eff}/E_g, and effective Poisson's ratio, ν^i, with respect to number of grains in unit area, n ($\nu_g=0.49$, $\nu_{gb}=0.499$, $K_{gb}/K_g=1.0$, $\mu_{gb}/\mu_g=0.1$)

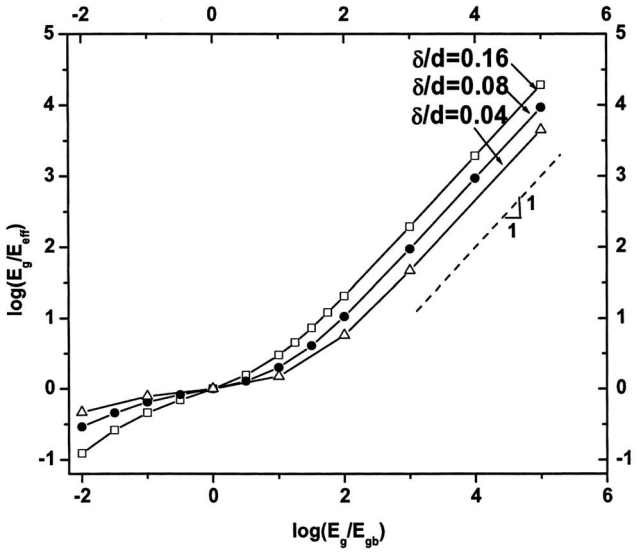

Fig. 6. Normalized Young's modulus, E_g/E_{eff}, as function of elastic mismatch, E_g/E_{gb} (for $\nu_g=\nu_{\text{gb}}=0.3$)

the edges of each cell, i.e., each edge is moved inward along its normal direction; (5) a unit square is cut at the center of this original tessellation; and (6) the grains and grain boundaries are discretized into a number of quadratic displacement triangular finite elements with reasonable element aspect ratios.

The Young's modulus and Poisson's ratio of the grains (grain boundaries) are denoted by E_g, ν_g ($E_{\text{gb}}, \nu_{\text{gb}}$). In terms of the displacement applied along the upper boundary, Δ, the boundary conditions are: $y=1$, $u_y=\Delta$; $x=0$ and $x=1$, $u_x=\sigma_{xy}=0$; $y=0$, $u_y=\sigma_{xy}=0$. For each of $m=500$ simulations, the boundary forces are calculated using the finite-element method, and the average stresses and strains in the homogenized plate are written as

$$\varepsilon^i_{xx}=0, \quad \varepsilon^i_{xy}=0, \quad \varepsilon^i_{yy}=\Delta/1 \tag{1a}$$

$$\sigma^i_{xx}=F^i_x/t, \quad \sigma^i_{xy}=0, \quad \sigma^i_{yy}=F^i_y/t \tag{1b}$$

where t=thickness of the plate, superscript "i"=ith Monte Carlo simulation, and F_x, F_y=reaction forces at boundaries (Fig. 4). The Young's modulus and Poisson's ratio are obtained by invoking Hooke's law for the homogenized plate

$$\begin{Bmatrix} \sigma^i_{xx}=F^i_x/t \\ \sigma^i_{yy}=F^i_y/t \\ \sigma^i_{xy}=0 \end{Bmatrix} = \frac{E^i}{(1+\nu^i)(1-2\nu^i)} \begin{bmatrix} 1-\nu^i & \nu^i & \\ \nu^i & 1-\nu^i & \\ & & \frac{1}{2}(1-2\nu^i) \end{bmatrix} \times \begin{Bmatrix} \varepsilon^i_{xx}=0 \\ \varepsilon^i_{yy}=\Delta \\ 2\varepsilon^i_{xy}=0 \end{Bmatrix} \tag{2}$$

which provides

$$\nu^i=\frac{1}{1+F^i_y/F^i_x}, \quad E^i=\frac{(1+\nu^i)(1-2\nu^i)}{\nu^i}\frac{F^i_x}{t\Delta} \tag{3}$$

The effective elastic moduli of the polycrystalline plate are defined as the average over m simulations of the moduli given by Eq. (3)

$$E_{\text{eff}}=\langle E^i\rangle, \quad \nu_{\text{eff}}=\langle \nu^i\rangle \tag{4}$$

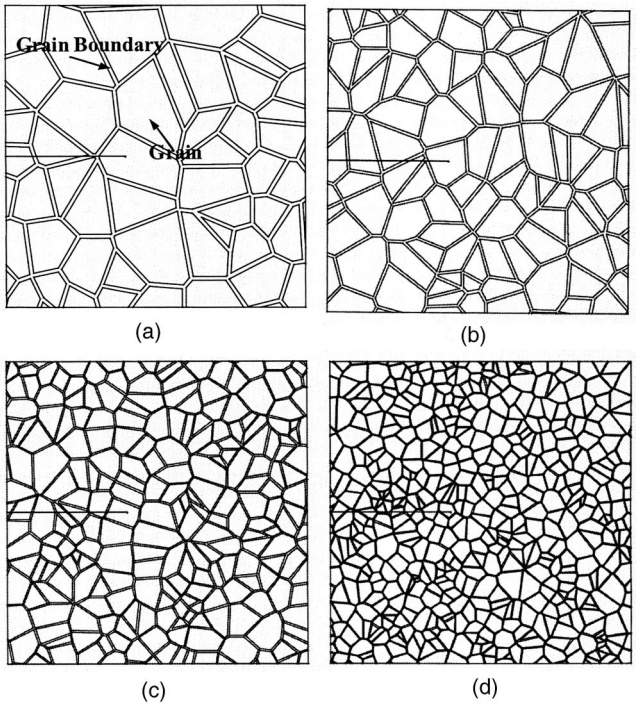

Fig. 7. Poisson–Voronoi tessellations of cracked polycrystalline plate: (a) $n=50$; (b) $n=100$; (c) $n=250$; and (d) $n=500$

The first illustrative example of the significant effects of elastic mismatch on effective moduli involves the parameters $\nu_g=0.49$, $\nu_{\text{gb}}=0.499$, $K_{\text{gb}}/K_g=1.0$, $\mu_{\text{gb}}/\mu_g=0.1$, where K=bulk modulus; and μ=shear modulus. This case corresponds to nearly incompressible grains and grain boundaries. The thickness of the grain boundary is set equal to 8% of the average linear dimension of the grains. Fig. 5 presents, for different values of the expected number of grains, n, the scatter of the Poisson's ratio and of the Young's modulus normalized with respect to the modulus of the grain. For all n, the effective moduli are $E_{\text{eff}}/E_g \approx 0.64$ and $\nu_{\text{eff}} \approx 0.49$.

Selected values of E_g/E_{eff} can be achieved by adjusting either the elastic moduli and/or the thickness of the grain boundaries. Fig. 6 shows the variations of E_g/E_{eff} for a wide range of E_g/E_{gb} (note the log-log scale), $\upsilon_g=\nu_{\text{gb}}=0.3$, and three values of normalized interphase thickness, $\delta/d \approx 0.04$, 0.08, and 0.16. It is observed that for $E_g/E_{\text{gb}} \gg 1$ the curves can be represented by either of the equations

$$\log\frac{E_g}{E_{\text{eff}}} \sim \log\frac{E_g}{E_{\text{gb}}} + C(\delta/d), \quad \frac{E_g}{E_{\text{gb}}} \gg 1 \tag{5a}$$

$$E_{\text{eff}} \sim C_1(\delta/d)E_{\text{gb}}, \quad \frac{E_g}{E_{\text{gb}}} \gg 1 \tag{5b}$$

indicating that the effective modulus is controlled by both the stiffness and the thickness of the grain boundaries. However, for modest values of E_g/E_{gb}, the influence of the interphase thickness is relatively minor, and the effective modulus is controlled by the modulus of the grain.

The trends of the micromechanical model are consistent with the asymptotic limits corresponding to spherical grains separated by more compliant thin ligaments (Batchelor and O'Brien 1977; Phan-Thien and Karihaloo 1982). These involve the dimension-

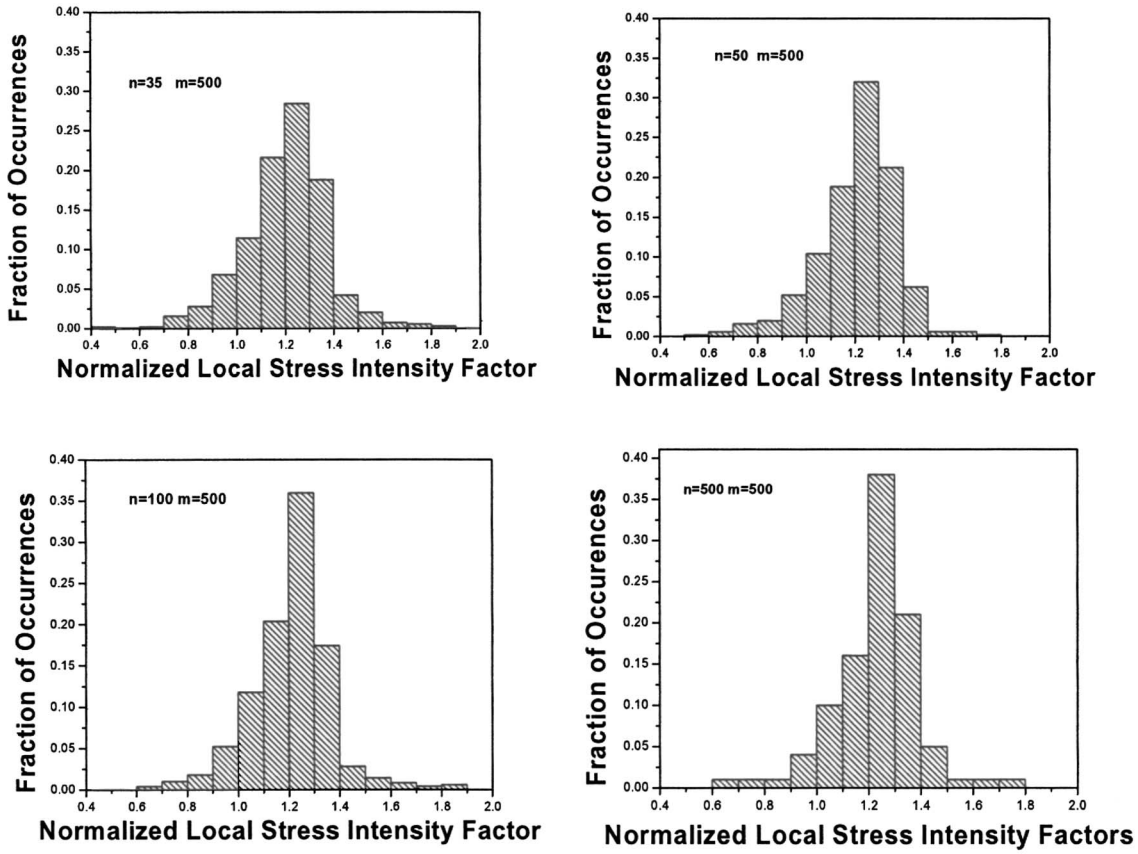

Fig. 8. Fraction of occurrences of normalized mode-I local stress intensity factors ($E_g/E_{\text{eff}} \approx 1.55, \nu_{\text{eff}} \approx 0.49$)

less variables $c_1=\delta/d$, $c_2=E_{\text{gb}}/E_g$, $C=c_2^{-2}c_1$, that were used by Rodin (2001) to develop an approximate analytical model of strength scaling in polycrystalline plates. For $C \gg 1$ the grains are practically rigid, and are separated by grain boundaries whose thickness and stiffness dictates the effective moduli. In contrast, for $C \ll 1$, the overall stiffness is controlled by the grains and is relatively insensitive to grain boundary thickness. According to Rodin, the following equations apply for these two limiting cases

$$E_{\text{eff}} \sim E_{\text{gb}} \log\left(\frac{d}{\delta}\right), \quad C \gg 1 \tag{6a}$$

$$E_{\text{eff}} \sim E_{\text{gb}} \log\left(\frac{E_g}{E_{\text{gb}}}\right)^2, \quad C \ll 1 \tag{6b}$$

Stress Intensity Factor Analyses

The crack-tip shielding/antishielding produced by the elastic mismatch between the grains and the grain boundaries is studied using the finite-geometry configuration shown in Fig. 2(a), where one edge of a cracked polycrystalline plate is subjected to a uniform displacement. Note that, strictly speaking, the crack in the polycrystalline plate is subjected to mixed mode loading; the apparent stress intensity factor, K_I^{ref}, produces local stress intensity factors, K_I^{loc}, K_{II}^{loc}. However, because the calculated results indicate that the Mode-II stress intensity factor is negligible, it will not be listed in subsequent figures and tables.

The effects of grain-grain boundary elastic mismatch, number of grains per unit area (Fig. 7), uniform distribution of crack-tip position within the single grain specimen, and random arrangement of the grains, are evaluated by performing $m=100-500$ Monte Carlo realizations. Fig. 8 shows the distributions of the normalized local stress intensity factor, $K_I^{\text{loc}}/K_I^{\text{ref}}$, which were calculated using singular elements (Barsoum 1977), for $\nu_g=0.49$, $\nu_{\text{gb}}=0.499$, $K_{\text{gb}}/K_g=1.0$, $\mu_{\text{gb}}/\mu_g=0.1$ ($E_g/E_{\text{eff}} \approx 1.55$, $\nu_{\text{eff}} \approx 0.49$). It is observed that $K_I^{\text{loc}}/K_I^{\text{ref}}$, whose average value is 1.2, is independent of the number of grains per unit area. The independence of the local stress intensity factor on the number of grains is maintained for larger ratios of elastic mismatch, as shown in Fig. 9 for the parameters $E_g/E_{\text{eff}} \approx 6.06$, $\nu_{\text{eff}} \approx 0.41$ ($\nu_g=0.2$, $\nu_{\text{gb}}=0.49$, $K_{\text{gb}}/K_g=0.15$, $\mu_{\text{gb}}/\mu_g=0.004$, and $\delta/d=0.08$).

The expected values, K_{avg}, and standard deviation, K_{sd}, of $K_I^{\text{loc}}/K_I^{\text{ref}}$ are listed in Table 2 together with those corresponding to the analytical model described next, for selected values of the parameters that quantify elastic mismatch. Remarkably, the shielding/antishielding of the crack tip that results from its random position is dominated by the ratio of elastic modulus of the single grain specimen to the effective elastic modulus of the surrounding ice machine. The lack of dependence on the number of grains suggests that $K_I^{\text{loc}}/K_I^{\text{ref}}$ could be approximated using the analytical micromechanical model shown in Fig. 10 (Wang and Ballarini 2003), as long as the shear modulus and Poisson's ratio of the $2a$-diameter circular inhomogeneity, μ_2, ν_2, are set equal to those of the single grain specimen (μ_g, ν_g), and the moduli of the surrounding material, μ_1, ν_1, are set equal to the previously calculated effective moduli of the uncracked polycrystalline plate (μ_{eff}, ν_{eff}). With the crack tip positioned at point $(w,0)$, and the plate loaded with a far field stress intensity factor set equal to the

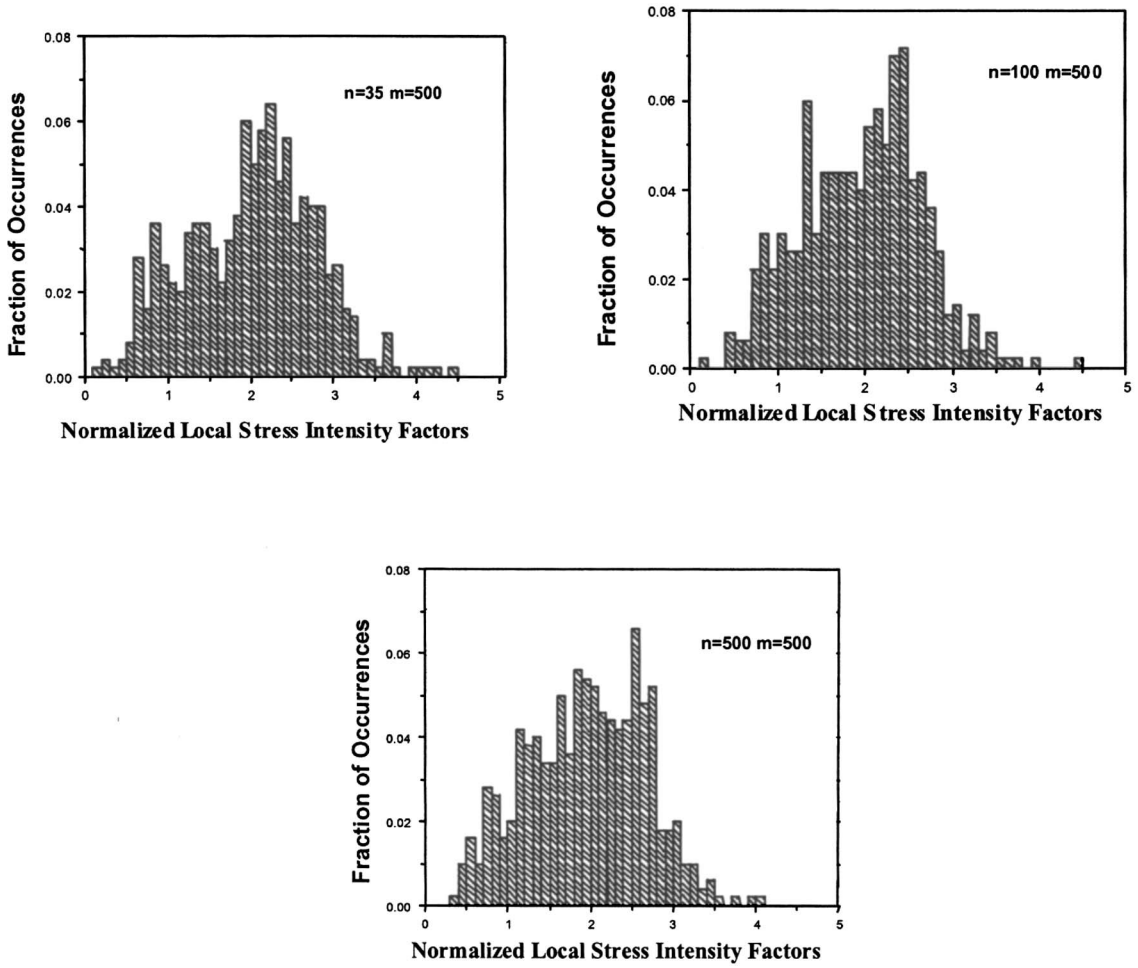

Fig. 9. Fraction of occurrences of normalized mode-I local stress intensity factors ($E_g/E_{\text{eff}} \approx 6.06, \nu_{\text{eff}} \approx 0.41$)

Table 2. Normalized Local Stress Intensity Factor ($\delta/d=0.08$)

E_g/E_{eff}	ν_g	ν_{eff}	n	m	K_{avg}	K_{sd}
1.55	0.49	0.49	approximate	—	1.24	0.06
			35	500	1.22	0.18
			50	500	1.21	0.17
			100	500	1.21	0.16
			500	500	1.23	0.17
1.47	0.2	0.34	approximate	—	1.15	0.03
			35	447	1.13	0.13
			100	280	1.13	0.11
			500	126	1.13	0.11
6.06	0.2	0.41	approximate	—	2.20	0.60
			9	300	2.01	0.83
			35	500	2.02	0.77
			100	500	1.96	0.68
			500	500	1.95	0.71
2.00	0.3	0.28	approximate	—	1.48	0.16
			50	500	1.42	0.18
			500	500	1.41	0.18
10.53	0.3	0.24	approximate	—	3.34	0.97
			50	500	3.02	1.00
			500	395	2.91	0.97
0.65	0.3	0.31	approximate	—	0.77	0.05
			50	500	0.73	0.11
			500	500	0.73	0.11

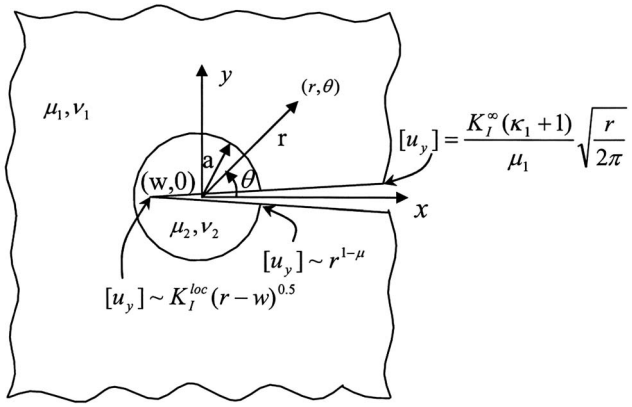

Fig. 10. Analytical model for local stress intensity factor of cracked polycrystalline plate

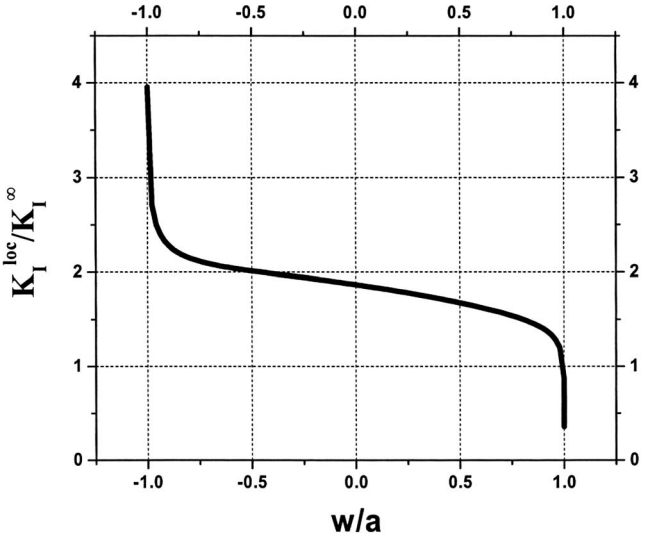

Fig. 11. Variation of normalized local stress intensity factor as crack traverses inhomogeneity calculated using approximate model ($E_g/E_{\text{eff}} \approx 3.05$, $\nu_g = 0.3$, $\nu_{\text{eff}} = 0.26$)

apparent stress intensity factor $K_I^{\infty} = K_I^{\text{ref}}$, the normalized local stress intensity factor can be written in the form

$$\frac{K_I^{\text{loc}}}{K_I^{\infty}} = f\left(\frac{w}{a}, \nu_1, \nu_2, \frac{\mu_1}{\mu_2}\right) \tag{7}$$

where f was calculated using the procedure summarized in the Appendix.

Fig. 11 shows the variation in the normalized local stress intensity factor as the crack tip traverses the inhomogeneity for the case $E_g/E_{\text{eff}} \approx 3.05$, $\nu_g = 0.3$, $\nu_{\text{eff}} = 0.26$. Consistent with the asymptotic behaviors of cracks approaching and penetrating biomaterial interfaces (Romeo and Ballarini 1995), the stress intensity factor is close to zero as it enters the inhomogeneity from the more compliant surrounding material, and continuously increases to infinity as it reaches the other side. This continuous increase demonstrates that the initial position of the crack tip determines the apparent fracture toughness of a polycrystalline plate with soft grain boundaries.

Application to Warm Lake Ice

The results of the micromechanical analyses can shed light on the large variation in apparent fracture toughness and effective elastic modulus data shown in Fig. 1(b) and Table 1.

A review of available ice data (Dempsey et al., 1999; Fletcher 1970), suggests that reasonable estimates of elastic modulus and Poisson's ratio of the grains, and effective Young's modulus, are 12 GPa, 0.3, and 4 GPa, respectively. The Monte Carlo procedure, in turn, provides $E_g/E_{\text{eff}} \approx 3$ and $\nu_{\text{eff}} = 0.26$. The ratio of three between the grains and the effective medium is achieved for selected values of δ/d, by adjusting the elastic constants of the grain boundaries E_{gb}, ν_{gb}. Table 3 presents, for $\delta/d = 0.04$, 0.08, 0.16 the expected value and standard deviation of normal-

Table 3. Normalized Local Stress Intensity Factor for Three Values of Normalized Interphase Thickness

E_g/E_{eff}	ν_g	ν_{eff}	n	m	K_{avg}	K_{sd}	G_{avg}	G_{sd}
			(a) $\delta/d = 0.04$					
3.05	0.30	0.26	approximate	—	1.86	0.30	1.13	0.39
			4	300	1.77	0.36	1.07	0.44
			9	300	1.77	0.32	1.06	0.36
			50	300	1.76	0.33	1.06	0.35
			(b) $\delta/d = 0.08$					
2.94	0.30	0.26	approximate	—	1.82	0.28	1.20	0.39
			4	300	1.70	0.35	1.08	0.44
			9	300	1.70	0.31	1.07	0.37
			50	300	1.70	0.30	1.06	0.35
			(c) $\delta/d = 0.16$					
3.01	0.30	0.28	approximate	—	1.83	0.28	—	—
			4	300	1.74	0.32	—	—
			9	300	1.73	0.33	—	—
			50	300	1.70	0.29	—	—
			100	300	1.72	0.29	—	—
			500	400	1.72	0.30	—	—

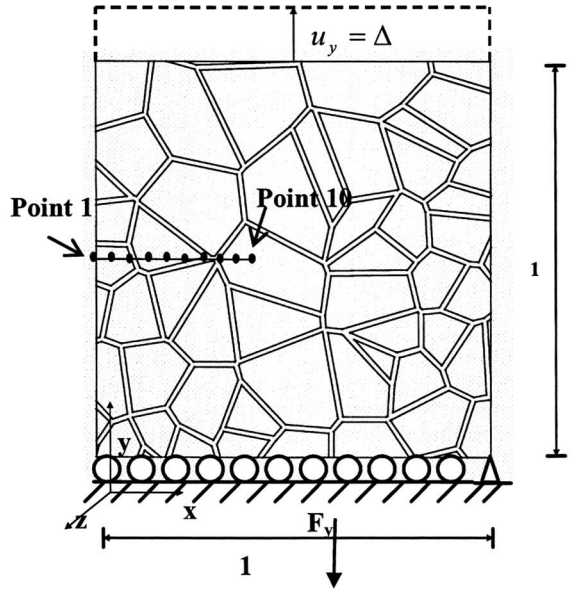

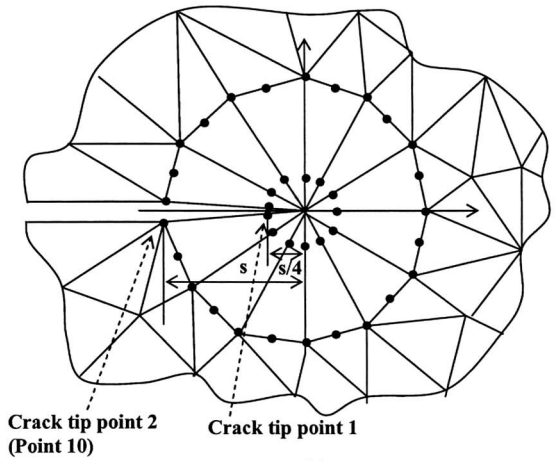

Fig. 12. Locations of points where crack opening displacements are calculated using Monte Carlo model: (a) Points 1–10; (b) Crack tip Points 1 and 2 (or *CTOD1* and *CTOD2*)

ized local stress intensity factor predicted by the Monte Carlo simulation and the analytical model. It is observed that the crack-tip parameter has a weak dependence on the thickness of the interphase.

As stated by Dempsey et al. (1999) ice grains are associated with an insignificant process zone, so that crack initiation within the grains can be characterized using the critical local stress intensity factor,$K_{\mathrm{Ic}}^{\mathrm{loc}}$. Neglecting the largest specimen datum, the apparent fracture toughness, $K_{\mathrm{Ic}}^{\mathrm{ref}}$, lies within the range 76–193 kPa $\mathrm{m}^{1/2}$, has an average value of 140 kPa $\mathrm{m}^{1/2}$, and has a −0.58 correlation with specimen size. Fig. 11 provides a possible explanation for why the lower and upper bounds of the apparent toughness data differ by a factor of ~2.5. If the crack tip was initially positioned just inside the single grain specimen, the normalized local stress intensity factor is ~1. However, if its initial position was closer to other side, the normalized stress intensity factor is ~2. The possibility that the apparent toughness is size independent, and merely reflects the variation in local stress intensity factor, is plausible.

Table 4. Normalized Crack Opening Displacements

Point	Average $\frac{\Delta_i}{(F_y/E_{\mathrm{eff}})}$	Standard deviation	Minimum	Maximum
1	0.51	0.047	0.35	0.63
2	0.47	0.044	0.32	0.58
3	0.43	0.040	0.29	0.54
4	0.39	0.039	0.24	0.50
5	0.35	0.035	0.20	0.46
6	0.30	0.032	0.20	0.38
7	0.26	0.030	0.16	0.33
8	0.20	0.027	0.13	0.27
9	0.13	0.025	0.067	0.20
10	0.0013	2.1E−0.4	6.8E−0.4	0.002
Tip point 1	6.4E−0.4	1.1E−0.4	3.4E−0.4	9.7E−0.4

This explanation is underscored by the crack opening displacements calculated using the finite-element method base Monte Carlo model of the cracked plate. Fig. 12 defines points at which the crack opening displacements, Δ_i, were calculated. These include ten points ($i=1,10$) that are uniformly distributed from the crack mouth (Point 1) to the crack tip region (Point 10), and an additional point very close to the crack tip The displacements are normalized with respect to F_y/E_{eff}, where F_y represents the reaction force along the bottom boundary of the unit square [Fig. 12(a)].

Table 4 presents the expected values, standard deviation, and range of the crack opening displacements for $n=50$. The maximum and minimum values at any given point along the crack differ by a factor of ~2, a result that may explain the inconsistencies in effective Young's modulus values obtained from crack opening displacement measurements at different points along the crack.

Conclusion

Crack-tip parameters in polycrystalline plates with soft grain boundaries are strong functions of crack-tip position. The ice-machine concept presented in this paper suggests that a fracture mechanics test of a polycrystalline plate provides the fracture toughness of the crystal that contains the crack tip. The remaining grains that surround this single crystal specimen form a compliant (ice) machine that is in series with the actual (metal) loading machine. Therefore proper interpretation of fracture mechanics experiments performed on such heterogeneous structures requires the use of micromechanical models that provide the stiffness of the ice machine, and correlate the critical value of the local stress intensity factor controlling crack initiation to the apparent fracture toughness. The need to calibrate the stiffness of the ice machine can be avoided by testing the single crystal directly in a metal machine.

Acknowledgments

Partial support for R. Ballarini was provided by the MTS Visiting Professorship in Geomechanics at University of Minnesota's Department of Civil Engineering. G. J. Rodin acknowledges the support of the National Science Foundation through Grant No.

CMS 0219839. The writers also thank John P. Dempsey of Clarkson University for useful discussions.

Appendix

The analytical model described in Fig. 10 was solved using the method of distributed dislocations and singular intergral equations (Wang and Ballarini 2003), summarized next. The zero traction condition along the crack surfaces is written as

$$\sigma_{\theta\theta} + i\tau_{r\theta} = 0 \quad w < x < \infty \tag{8}$$

The stress combination in Eq. (8) produced at any point x by discrete dislocations at points t inside and outside the circular inhomogeneity can be written symbolically as

$$\sigma_{\theta\theta} + i\tau_{r\theta} = \frac{2B_1}{x-t} + B_1K_{11}(x,t) + B_2K_{12}(x,t) \quad a < x < \infty \tag{9}$$

$$\sigma_{\theta\theta} + i\tau_{r\theta} = \frac{2B_2}{x-t} + B_2K_{21}(x,t) + B_1K_{22}(x,t) \quad w < x < a \tag{10}$$

where B_1 and B_2 are proportional to the magnitude of the displacement discontinuity associated with the dislocations outside and inside the inhomogeneity, respectively.

By introducing the dislocation densities

$$b_i(t) = \frac{\mu_i}{\pi i(\kappa_i+1)}\frac{\partial\{[u_x]+i[v_y]\}}{\partial t} = \frac{\mu_i}{\pi(\kappa_i+1)}\frac{\partial[v_y]}{\partial t} \tag{11}$$

the traction boundary condition along the crack surfaces can be written in the form of the coupled singular integral equations

$$\int_a^\infty \frac{2b_1(t)}{x-t}dt + \int_a^\infty K_{11}(x,t)b_1(t)dt + \int_w^a K_{12}(x,t)b_2(t)dt = 0 \quad x > a$$

$$\int_w^a \frac{2b_2(t)}{x-t}dt + \int_w^a K_{21}(x,t)b_2(t)dt + \int_a^\infty K_{22}(x,t)b_1(t)dt = 0 \quad w < x < a \tag{12}$$

The kernels are defined as

$$K_{ij}(x,t) = K_{ijs}(x,t) + K_{ijf}(x,t), \quad i,j = 1,2$$

$$K_{11s}(x,t) = \left[-2P_1 + (P_2-P_1)\frac{a^2}{x^2}\right]\frac{1}{(a^2/x-t)} + \left[-2P_1\frac{a^2}{x^5}(x^2+2a^2)\right]\frac{(x^2-a^2)}{(a^2/x-t)^2} + \left[-2P_1\frac{a^4}{x^6}\right]\frac{(x^2-a^2)^2}{(a^2/x-t)^3}$$

$$K_{11f}(x,t) = \frac{\left[-\left(2+\frac{a^2}{x^2}\right)P_1 + \frac{a^2}{x^2}(M_1-1)\right]}{t}$$

$$K_{12s}(x,t) = \left[2Q_1 + (Q_1-Q_2)\frac{a^2}{x^2}\right]\frac{1}{x-t} + \frac{[Q_2-Q_1]}{x}\frac{(x^2-a^2)}{(x-t)^2}$$

$$K_{12f}(x,t) = \left[\frac{N_1-N_2}{x} + \frac{2N_3t}{x^2} + \frac{2N_1a^2}{x^3}\right]$$

$$K_{21s}(x,t) = \left[-2Q_3 + (Q_4-Q_3)\frac{a^2}{x^2}\right]\frac{1}{(a^2/x-t)} + \left[-2Q_3\frac{a^2}{x^5}(x^2+2a^2)\right]\frac{(x^2-a^2)}{(a^2/x-t)^2} + \left[-2Q_3\frac{a^4}{x^6}\right]\frac{(x^2-a^2)^2}{(a^2/x-t)^3}$$

$$K_{21f}(x,t) = \frac{4N_4t}{a^2} - \frac{Q_3+Q_4}{x} + \frac{2(N_4+N)t}{x^2} - \frac{2Q_3a^2}{x^3}$$

$$K_{22s}(x,t) = \left[2P_3 + \frac{a^2}{x^2}(P_3-P_4)\right]\frac{1}{x-t} + \frac{P_4-P_3}{x}\frac{(x^2-a^2)}{(x-t)^2}$$

$$K_{22f}(x,t) = \frac{\left[2M_2 + \frac{a^2}{x^2}(M_2+M-P_4)\right]}{t} \tag{13}$$

involving the constants

$$P_1 = \frac{\beta-\alpha}{1+\beta}, \quad P_2 = \frac{\alpha+\beta}{\beta-1}, \quad M_1 = \frac{(1+\alpha)(1-\alpha)}{(1+\alpha-2\beta)(1-\beta)}$$

$$P_3 = \frac{1+\alpha}{1-\beta}, \quad P_4 = \frac{1+\alpha}{1+\beta}, \quad M = \frac{1+\alpha}{1+\alpha-2\beta}, \quad M_2 = M\frac{\alpha-\beta}{1-\beta}$$

$$Q_1 = \frac{1-\alpha}{1+\beta}, \quad Q_2 = \frac{1-\alpha}{1-\beta},$$

$$N_1 = \frac{(1-\alpha)(\beta-\alpha)}{(1+\alpha)(1+\beta)}, \quad N_2 = \frac{(1-\alpha)(\beta+\alpha)}{(1+\alpha)(1-\beta)},$$

$$N_3 = -\frac{(1-\alpha)(\alpha-\beta)}{(1-\beta)(1+\alpha-2\beta)}$$

$$Q_3 = \frac{(\alpha-\beta)}{(1-\beta)}, \quad Q_4 = \frac{(\alpha+\beta)}{(1+\beta)}, \quad N = -\frac{(\beta-\alpha)}{(1+\alpha-2\beta)},$$

$$N_4 = Q_3 \times N \tag{14}$$

The first integral in each of Eqs. (12) contains a Cauchy kernel, while the K_{ij} are combinations of regular kernels K_{ijf} and generalized kernels K_{ijs}, the latter being unbounded as x and t approach a simultaneously. The integral equations were solved using a technique that relies on properties of Jacobi polynomials, which rigorously incorporates the behavior of the dislocation densities at all singular points. The procedure produces function f defined in Eq. (7).

References

Barnes, P., Tabor, D., and Walker, J. C. F. (1971). "The friction and creep of polycrystalline ice." *Proc. R. Soc. London, Ser. A*, 324, 127–155.
Barsoum, R. S. (1977). "Triangular quarter-point elements as elastic and

perfectly-plastic crack tip elements." *Int. J. Numer. Methods Eng.*, 11, 85–98.

Batchelor, G. K., and O'Brien, R. W. (1977). "Thermal or electrical conduction through a granular material." *Proc. R. Soc. London, Ser. A*, 355, 313–333.

Dempsey, J. P., Defranco, S. J., Adamson, R. M., and Mulmule, S. V. (1999). "Scale effects on the *in-situ* tensile strength and fracture of ice. Part I: Large grained freshwater ice at spray lakes reservoir, Alberta." *Int. J. Fract.*, 95, 325–345.

Fletcher, N. H. (1970). *The chemical physics of ice*, Cambridge University Press, Cambridge, U.K.

Gandhi, C., and Ashby, M. F. (1979). "Fracture-mechanism maps for materials that cleave: F. C. C., B. C. C., and H. C. P. metals and ceramics." *Acta Metall.*, 27, 1565–1602.

Mullen, R. L., Ballarini, R., and Yin, Y. (1997). "Monte-Carlo simulation of effective elastic constants of polycrystalline thin films." *Acta Mater.*, 45(6), 2247–2255.

Phan-Thien, N., and Karihaloo, B. L. (1982). "Effective moduli of particulate solids." *Z. Angew. Math. Mech.*, 62, 183–190.

Rodin, G. J. (2001). "On fracture of warm ice." *Proc., IUTAM Symp. on Scaling Laws in Ice Mechanics and Ice Dynamics*, Fairbanks, Alaska.

Romeo, A., and Ballarini, R. (1995). "A crack very close to a bimaterial interface." *J. Appl. Mech.*, 62, 614–619.

Voronoi, G. (1908). "Nouvelles applications des parametres continus a la theorie des formes quadratiques, deuxieme memoire, recherches sur les parallell edres primitifs." *J. Reine Angew. Math.*, 134, 198–287.

Wang, Y., and Ballarini, R. (2003). "A long crack penetrating a circular inhomogeneity." *Meccanica*, 38, 579–593.